Lasing Yb 3+ in crystals with a wavelength dependence anisotropy displayed from La 2 CaB10O19

A Brenier, Y Wu, J Zhang

Lasing Yb^{3+} in crystals with a wavelength dependence anisotropy displayed from $La_2CaB_{10}O_{19}$

A. BRENIER[1*], Y. WU[2], J. ZHANG[2], Y. WU[2,3]

[1]Laboratoire de Physico-Chimie des Matériaux Luminescents, CNRS UMR 5620, Université Claude Bernard Lyon 1, 10 rue Ada Byron, 69622 Villeurbanne, France

[2]Key Laboratory of Functional Crystals and Laser Technology, Technical Institute of Physical Chemistry, Chinese Academy of Sciences, Beijing 100080, China

[3]Graduate University of Chinese Academy of Sciences, Beijing 100049, China

[*] e-mail: alain.brenier@univ-lyon1.fr

Abstract: We report spectroscopic and laser properties for propagation directions outside the principal axes of Yb^{3+}-doped low symmetry laser crystals with a special devotion to the wavelength dependence anisotropy. We illustrate our talk with experimental data in the 900-1075 nm range of wavelengths from the Yb^{3+}: $La_2CaB_{10}O_{19}$ monoclinic crystal excited under laser diode pumping at 975 nm. This study, which makes easier the realization of Yb^{3+} lasers with an efficient free running at the wavelength having the highest emission intensity or at a specified wavelength, or emitting two-frequencies with a specified frequency difference, is of promising interest for applications.

1. Introduction

Yb^{3+} lasing offers much advantages for coherent light generation near 1 µm wavelength. The $4f^{13}$ electronic configuration of the Yb^{3+} ion located in a host matrix results in a very favourable energy level scheme constituted of only one excited sate, $^2F_{5/2}$.[1] The possible low quantum defect, around 10% or less, between pump and laser photons reduces the heat generated inside the material and then its thermal deformation[2,3]. Excited-state absorption and up-conversion losses, which are traditional factors limiting the laser efficiency, cannot occur for Yb^{3+} centres. Regarding absorption, selective pumping from laser InGaAs diodes has led to efficient, powerful and compact devices since more than a decade. This tendency is expected to be confirmed in the future, due to novel vertical-cavity surface-emitting lasers (VCSEL) recently used with success in a solid-state laser[4]. Laser beam quality is also making progress, let us cite the thin disc technique[5,6]. A new field (so called micro-solid state photonics) in the fabrication of anisotropic laser materials has arisen recently: the elaboration of anisotropic ceramics by using a magnetic field to orientate the rare-earth doped micro-grains[7]. The other asset of lasing Yb^{3+} instead of Nd^{3+} is due to its broadband emission which is a consequence of the electron-phonon coupling. Laser emission tunable over tens of nanometers can be obtained or ultra-short pulses can be generated[6].

Concerning the applications, they are numerous: material processing, medical, laser nuclear fusion, military projects…

When the host is anisotropic it is desirable to choose the propagation direction which allows polarized lasing with the highest emission cross-section, but not necessarily. For example the usual polarization for lasing the Yb^{3+} doped $KGd(WO_4)_2$ crystal is the N_m principal axis[8], but lasing with the N_g polarisation can be beneficial for compact Q-switched lasers[9] due to a highest stored energy if the emission cross-section is lower[10]. More, for one

given direction, two polarized modes can propagate, each with its own frequency. A two-frequency laser was realized with a Yb^{3+} doped $KGd(WO_4)_2$ crystal oriented in the N_m-N_g principal plane[11,12]. The beatnote can modulate the photocurrent induced inside a photomixer associated with an antenna[13-15], constituting an indirect source of THz radiations. Frequency conversion in a nonlinear optical crystal (GaP, $LiNbO_3$, $ZnGeP_2$, GaSe…) can also be used[16-18]. Terahertz waves, which are safe for human on the contrary to X-rays, have a huge potential for non-destructive imaging of concealed objects and free-space communications[19-,21].

Now the stumbling block for the "best" propagation is that it is not a straightforward task to measure or predict the whole spatial distribution of the fluorescence (the same for absorption). We have to remind that generally absorption and fluorescence extrema do not coincide with the three principal X, Y, Z axes of the indices ellipsoid. So, usual spectroscopic X, Y, Z polarization measurements are not sufficient for a full description. Regarding absorption these considerations (pleochroism) were recognized more than a century ago[22-24]. In the field of laser materials, only recently a few authors devoted efforts to this aspect: first with the monoclinic Nd^{3+}: $YCa_4O(BO_3)_3$[25,26], then with Nd^{3+}: $La_2CaB_{10}O_{19}$[27]. A refined effect for propagation along the optics axis is even proposed[28]. However up to now Yb^{3+}-doped laser crystals have escaped this research despite of their fame. Let us cite the monoclinic $YCa_4O(BO_3)_3$, $GdCa_4O(BO_3)_3$, $Li_6Y(BO_3)_3$, $KGd(PO_3)_4$ and surprisingly $KGd(WO_4)_2$ and $KY(WO_4)_2$. We report here a research in this topic with a special attention to the wavelength dependence. We illustrate our talk with spectroscopic and laser results measured with the Yb^{3+}: $La_2CaB_{10}O_{19}$ monoclinic crystal.

2. Experimental methods

A good quality Yb^{3+}-doped $La_2CaB_{10}O_{19}$ single crystal with size of 40×15×20 mm^3 was grown with Li_2O-CaO-B_2O_3 flux[29] using the top-seeded solution growth (TSSG) method in a

vertically cylindrical resistance heated furnace. The starting material was prepared with a solid-state reaction method. Analytical grade La_2O_3, Yb_2O_3, $CaCO_3$, Li_2CO_3 and H_3BO_3 were weighed according to the molar ratio of 0.85:0.15:2:2.3:28. Being ground and mixed thoroughly, the mixture was preheated at 450^oC for 12h to decompose the H_3BO_3, and then the mixture was ground again and sintered at 900 ^oC for 24 h in a Platinum crucible. Owing to the growth anisotropy of the Yb: $La_2CaB_{10}O_{19}$ crystal, the seed direction is most important in growth process for high quality Yb: $La_2CaB_{10}O_{19}$ crystals. In order to obtain large, transparent and nearly defect-free region, we selected the seed growth direction slightly deviating from [110] direction[30]. During the growth, the rotation rate was 9~15 rpm and the temperature-lowering rate was less than 0.5^oC/day. After 2 months growth cycle, the crystal was cooled down to room temperature at rate of 20-40^oC/h. A colorless, transparent and rhomboid shaped crystal was obtained.

The Yb^{3+} doping of the $La_2CaB_{10}O_{19}$ samples used in the spectroscopic and laser experiments was 15%, corresponding to 2.77 10^{20} ions/cm^3 concentration measured by inductively coupled plasma atomic emission spectroscopy (ICP-AES).

The absorption spectra of the different Yb^{3+}-doped $La_2CaB_{10}O_{19}$ samples were recorded with a Lambda 900 Perkin Elmer spectrophotometer. The Yb^{3+} fluorescence was excited at 953 nm from an hydrogen cell Raman shifter pumped at 532 nm with a BM Industries frequency doubled pulsed Nd:YAG laser. The fluorescence was detected with a R1767 Hamamatsu photomultiplier through a Jobin-Yvon HRS2 monochromator equipped with a 1 μm blazed grating. The fluorescence lifetime has been measured with a digital Lecroy oscilloscope.

The lengths of the Yb^{3+}:$La_2CaB_{10}O_{19}$ samples used in the laser experiments were close to 3 mm. Their two faces were anti-reflection coated near 1040 nm. Their laser performance was evaluated in a free-running operation. The samples were located inside a 4.2 cm length plano-

concave laser cavity. The rear mirror was a plane dichroic mirror coated for high reflexion in the 1020-1080 nm range of wavelengths and high transmission at 975 nm pumping wavelength. The concave output coupler had a radius of curvature of 5 cm and a reflectance of 98%. The laser crystal was mounted in a copper heat sink and located at a few mm from the rear mirror. The temperature of the water cooled, copper heat sink was maintained at 15^{o}C. The pumping beam was provided by a fiber-coupled laser diode from LIMO (N. A. = 0.22, fiber core diameter: 200 μm). The pump was focused into the laser crystal by two 60 mm focal length doublets, the diameter of the focal point being about 220 μm.

3. Fundamentals

The electromagnetic wave properties and in particular the spectroscopic properties (absorption and emission cross-sections in cm^2 or equivalently absorption and amplification (by stimulated emission) coefficients in cm^{-1}) of a laser material are fully obtained in any direction of propagation for the two orthogonal polarized modes from the linear (symmetric) permittivity tensor:

$$\varepsilon = \varepsilon_0 \left(\varepsilon' + i\varepsilon'' \right) \qquad (1)$$

through Maxwell equations. In the so-called X, Y, Z dielectric frame (where equation (1) is written) the real part, related to the refraction indices, is diagonal but the imaginary part is not (it is diagonal in a rotated X', Y', Z' frame). So its elements contain six independent parameters related to spectroscopy and to be determined experimentally. Three of these parameters are linked to the strength of three mutually orthogonal electric dipoles aligned with the X', Y' Z' axis and responsible for the electronic transitions of the lasing centres. The other three parameters describe the 3-D rotation making the X', Y', Z' → X, Y, Y frame transfer. For example the X-polarized absorption coefficient k_x (or amplification coefficient) is simply:

$$k_x = C\,\sigma_x = \frac{2\pi}{n_x \lambda}\varepsilon''_{xx} \qquad (2)$$

where C is the dopant concentration (ions/cm3) and σ_x the X-polarized absorption/emission cross-section.

Propagation modes are found inserting $\mathbf{E}\exp(i\,\mathbf{k}.\mathbf{r} - \omega\,t)$ solutions in Maxwell equations and the result is the well-known Fresnel equation. Due to the transverse behaviour of the dielectric displacement vector $\mathbf{D}$, it is convenient to work and express the permittivity tensor in a frame x_1, x_2, x_3 whose third axis x_3 is parallel to the propagation direction $\mathbf{k}(\theta,\varphi)$ defined par the polar and azimuthal angles (θ, ϕ):

$$\underline{\underline{\varepsilon}}(\theta,\varphi) = S(\theta,\varphi)\,\varepsilon\,S^{T}(\theta,\varphi) \qquad (3)$$

where $S(\theta,\varphi)$ is the 3-D rotation making the (X, Y,Z)→(x_1, x_2, x_3) frame transfer. Let us use the notations:

$$\delta_{11} = \underline{\underline{\varepsilon}}_{11}\underline{\underline{\varepsilon}}_{33} - \underline{\underline{\varepsilon}}_{13}\underline{\underline{\varepsilon}}_{31} \qquad \delta_{12} = \underline{\underline{\varepsilon}}_{12}\underline{\underline{\varepsilon}}_{33} - \underline{\underline{\varepsilon}}_{13}\underline{\underline{\varepsilon}}_{32}$$

$$\delta_{21} = \underline{\underline{\varepsilon}}_{21}\underline{\underline{\varepsilon}}_{33} - \underline{\underline{\varepsilon}}_{23}\underline{\underline{\varepsilon}}_{31} \qquad \delta_{22} = \underline{\underline{\varepsilon}}_{22}\underline{\underline{\varepsilon}}_{33} - \underline{\underline{\varepsilon}}_{23}\underline{\underline{\varepsilon}}_{32} \qquad (4)$$

The Fresnel equation is the characteristic equation of a 2-dimension eigenvalue problem whose solutions are the two wavenumbers given by the following formula[31]:

$$k_a(\theta,\varphi) = \omega\left[\frac{\mu_0}{2\underline{\underline{\varepsilon}}_{33}}\left\{(\delta_{11}+\delta_{22}) + \left[(\delta_{11}-\delta_{22})^2 + 4\delta_{12}\delta_{21}\right]^{1/2}\right\}\right]^{1/2} \qquad (5)$$

$$k_b(\theta,\varphi) = \omega\left[\frac{\mu_0}{2\underline{\underline{\varepsilon}}_{33}}\left\{(\delta_{11}+\delta_{22}) - \left[(\delta_{11}-\delta_{22})^2 + 4\delta_{12}\delta_{21}\right]^{1/2}\right\}\right]^{1/2} \qquad (6)$$

On the contrary to absorption, stimulated emission is generally not measured directly but through fluorescence intensity given in photons/s by the detectors. The drawback is that no physical basis implies that the fluorescence intensity could be proportional to the imaginary part of the permittivity tensor but expressions such as (2) show that the emission cross-section does. So, the last step in order to use (5) and (6) is to connect the emission cross-section σ_e with the measured fluorescence intensity I. This can be accomplished with McCumber relations[32] including the radiative lifetime τ_{rad} of the laser emitting level. The connection is:

$$\sigma_e(\mathbf{k}_p,\lambda) = \frac{\lambda^4}{n^2(\mathbf{k}_p,\lambda)\, c\, \tau_{rad}} \; \frac{I(\mathbf{k}_p,\lambda)}{\sum_p \iint_{4\pi} d\Omega_k \int I(\mathbf{k}_p,\lambda) d\lambda} \qquad (7)$$

where p=a or p=b represents the mode in the (θ,ϕ) direction of propagation with $\mathbf{k}_p(\theta,\varphi)$ as its wave-vector, c is the speed of light in vacuum, $d\Omega_k$ is the elementary solid angle in the **k**-space to be integrated over 4 π ster. and λ is the fluorescence wavelength. Comparison of expressions (2) and (7) leads to the interesting result that the imaginary part of the diagonal elements of the permittivity tensor is not proportional to the fluorescence intensity I, but that the amplification coefficient in a given propagation direction is proportional to $\frac{\lambda^4}{n^2} I$. This is crucial for describing the wavelength dependence.

Because no spectroscopic or laser data are available from triclinic laser crystal, we illustrate now our talk with Yb^{3+}-doped monoclinic crystals. The real part (diagonal) of the tensor (1) is supposed to be known from the measured refractive indices at the wavelengths of interest with the help of Sellmeier formula. Let us explicit the case where the principal axis X'Y'Z' of the imaginary part of the permittivity tensor and the XYZ ones are rotated with an

angle θ_0 around their common Y=Y' principal axis. A nondiagonal term ε''_{xz} appears if we express ε''_{ij} in the XYZ frame from its diagonal expression $\varepsilon''_{i'j'}$ in the X'Y'Z' frame:

$$\begin{bmatrix} \varepsilon''_{xx} & 0 & \varepsilon''_{xz} \\ 0 & \varepsilon'_{yy} & 0 \\ \varepsilon''_{xz} & 0 & \varepsilon''_{zz} \end{bmatrix} = \begin{bmatrix} \cos\theta_0 & 0 & \sin\theta_0 \\ 0 & 1 & 0 \\ -\sin\theta_0 & 0 & \cos\theta_0 \end{bmatrix} X \begin{bmatrix} \varepsilon''_{x'x'} & 0 & 0 \\ 0 & \varepsilon''_{y'y'} & 0 \\ 0 & 0 & \varepsilon''_{z'z'} \end{bmatrix} X \begin{bmatrix} \cos\theta_0 & 0 & -\sin\theta_0 \\ 0 & 1 & 0 \\ \sin\theta_0 & 0 & \cos\theta_0 \end{bmatrix}$$

(8)

Inspection[27] of ε''_{ij} reveals that the θ_0 angle can be obtained from the formula:

$$\mathrm{tg}(2\theta_0) = \frac{2\varepsilon''_{xz}}{\varepsilon''_{zz} - \varepsilon''_{xx}} \qquad (9)$$

In short, the four parameters $\varepsilon''_{ij}(\lambda)$ will be determined as a numerical adjustment of the $k_{a,b}$ values (5) and (6) with spectroscopic data recorded at least in four polarizations. Generally the three X, Y, Z polarizations are from two directions of propagation chosen among X($\theta=\pi/2$, $\phi=0$), Y($\theta=\pi/2$, $\phi=\pi/2$), Z($\theta=0$) and in these cases equations (5) and (6) reduce to equation (2) and other similar ones. The fourth polarization, in the XZ plane, is the one of the extraordinary wave propagating in the XZ principal plane ($\phi=0$) at a given θ polar angle.

4. Spectroscopic results

The $La_2CaB_{10}O_{19}$ crystal is monoclinic biaxial with C_2 space group. Some physical properties have been established experimentally: mechanical, thermal, laser-induced damage threshold, linear and nonlinear optical properties[33]. The electronic and optical properties have been evaluated theoretically from the full potential linear augmented plane wave method.[34] Co-doping with Nd^{3+}-Yb^{3+} leads to interesting temperature anomalies in emission spectra[35].

The 2-fold b crystallographic axis of the $La_2CaB_{10}O_{19}$ crystal is parallel to the Y-principal axis with the refractive indices order: $n_X<n_Y<n_Z$, leading to the knowledge of the wavelength dependence of the real part ε'_{ij} and on another hand, from a classical optics formula, to the polar angle of the directions of the two optics axis lying in the XZ-plane: $V_z=\pm 8.6°$. Now it is easy to check from inspection of expressions (5) and (6) that the a-modes correspond in any direction of propagation to the highest refractive index. In other words $n_a(\theta, \phi) > n_b(\theta, \phi)$. A consequence useful below is that for a propagation limited to the XZ-principal plane in the θ-direction, the extraordinary waves are described by the a-modes if $|\theta| > |V_z|$ and by the b-modes if $|\theta| < |V_z|$ (the opposite for the ordinary waves).

To determine the three diagonal elements of the imaginary part ε''_{ij} of the Yb^{3+}:$La_2CaB_{10}O_{19}$ crystal, samples with the X, Y, Z orientations have been cut and polished, both for absorption and emission. The X, Y, Z polarized absorption and emission spectra are given in Fig. 1 (a) and 2 (a) respectively, in the 900-1075 nm range of wavelengths. Outside this range, a weak green emission was observed, but only under strong focusing of a continuous pump beam. We attribute it originating from unavoidable Er^{3+} traces in the crystal and we have no evidence of blue-green emission (near 490 nm) originating from possible aggregation of the Yb^{3+} ions such as ion pairs. We believe that it has no influence on the present study. Likewise, we have found a single exponential decay time (1.037 ms) of the fluorescence attributed to Yb^{3+} ions located in the regular La^{3+} sites, and we have no evidence of Yb^{3+} ions located elsewhere involving a non-stoichiometric composition, for example located in the Ca^{2+} position.

The off-diagonal element ε''_{xz} requires crystals oriented for propagation in the XZ-principal plane and we have used polar angles ±37° or close (the reason is that theses directions phase-match the second harmonic generation of the fundamental 1040 nm laser

wave and are useful for self-frequency doubling). Spectra recorded in extraordinary polarization with orientations almost symmetrical in respect of the Z-axis, -37.4° and +38.1°, are quite different (Fig. 3 (a) for absorption and 3 (b) for emission). This is the signature of the spatial distribution rotation of the spectroscopic properties around the 2-fold b (Y) axis: the XZ-plane is no more a symmetry plane as it is for higher crystal symmetries (orthorhombic and higher ones). The wavelength dependence of the fourth spectroscopic ε''_{xz} parameter, obtained by numerical matching the expression (5) (because the e-wave with $|\theta| > |V_z|$ correspond to the a-modes) with the spectra, is given in Fig. 1 (b) and 2 (b) for absorption and emission respectively. In Fig. 1 (b) the ε''_{xz} parameter is calculated for a 2.77 10^{20} ions/cm^3 (15% Yb^{3+}) doped absorbing sample and in Fig. 2 (b) for an excited-state population of an amplifying sample fixed at one tenth of this concentration, which is a reasonable value obtained under focused laser diode pumping. The rotation angle θ_0 (from equation (9) of the X', Y', Z' frame is reported in the same figures for some selected wavelengths corresponding to peaks in the spectra. We can notice a profound wavelength dependence of the rotation, both in sign and amplitude.

Once we have determined the wavelength dependence of the four ε''_{ij} parameters, it is meaningful to fixe a wavelength of interest and to build up the whole spatial distribution (absorption or emission) with the help of (5) and (6). We illustrated this build up for the stimulated emission cross-section at 1029.6 nm because this emission peak is close to an observed lasing wavelength (see section below). The result, obtained including in expression (7) the value of the radiative lifetime: 955 μs (this lifetime is well approximated by the one measured with a weak (3%) concentrated sample), is given in color scale in Fig. 4 (a) and 5 (a) for the a and b-modes respectively, the (θ, ϕ) direction of propagations being marked out by the orthogonal projection on the XZ principal plane of the (θ, ϕ) direction unit vector. The

distribution rotation around the Y-axis is clearly seen for the a-mode. This mode reduces to the extraordinary waves if we limit to propagation directions inside the XZ-principal plane (directions represented by the circle with radius one in Fig. 4 (a)) and with a polar angle $|\theta| > |V_z| = 8.6°$. This is why the rotation is seen idendically if we report radially in polar coordinates (Fig. 4 (b)) the fluorescence intensity (arbitrary units) with the extraordinary polarization. A circular distribution is of course obtained for the ordinary wave (Fig. 5 (b)).

5. Lasing

In order to test the influence on lasing of the spectroscopic properties rotation around the b (Y) axis, $Yb^{3+}:La_2CaB_{10}O_{19}$ crystals oriented for various propagation directions in the XZ principal plane ($\phi=0°$) were cut. In particular, to be close to conditions leading to spectra in Fig. 3 (a) and (b), two crystals with the polar angles $\theta = -37.4°$ and $\theta = +37.0°$ were prepared with a laser quality. Lasing was obtained under diode pumping in both polarizations: ordinary mode (Y-polarized) and extraordinary mode (XZ-plane polarized). A slight adjustment of the laser cavity alignment with the help of a polarizer allowed to choose lasing in ordinary mode or in the extraordinary one due to the walk-off angle inside the crystal. The spectral dependence of the laser waves are represented in Fig. 6 (a) and (b) for the two crystals oriented with $\theta = -37.4°$ and $\theta = +37.0°$ respectively. As expected from its spectroscopic properties symmetry around the Y-axis exhibited in Fig. 5 (b), the ordinary mode has lasing at the same wavelength (1044.7 nm) for the two crystals. On the contrary, lasing of the extraordinary mode occurs close to 1044.3 nm for the $\theta = -37.4°$ oriented crystal and at 1032.9 nm for the $\theta = +37.0°$ oriented crystal. Such a difference (3.2 THz) is in full accordance with the spectroscopic properties rotation around the Y-axis of this mode exhibited in Fig. 4 (a) and (b). It is also in agreement with the two emission spectra in Fig. 3 (b) where we can see that the emission peaks at long wavelengths are shifted.

Theses experiments show that the frequency difference of the two lasing modes is propagation direction dependent. This result can be explained on the basis of several orientations versus the frame of the refractive indices of the X' and Z' electric dipoles responsible for the spectroscopic properties and more, on the basis of the wavelength dependence of their orientation. The lasing wavelengths can be predicted knowing the direction dependence of the laser gain inside the laser cavity in addition with the cavity losses.

6. Conclusion

The realization of Yb^{3+} lasers with an efficient free running at the wavelength having the highest emission intensity or at a specified wavelength, or emitting two-frequencies with a specified frequency difference, is of promising interest for applications. Then tuning the wavelength around the free-running one with a prism, a grating or volume Bragg grating should be easier. This purpose can be achieved from a deep understanding of the linear optical properties of low symmetry laser crystals, including absorption or emission. Generally in these crystal absorption and emission extrema do not coincide with the principal axis of the well-known dielectric frame. Our talk is illustrated with spectroscopic and laser results measured with the Yb^{3+}: $La_2CaB_{10}O_{19}$ monoclinic crystal. Once the parameters involved in spectroscopy are determined from experimental data (four parameters in the monoclinic case included in the imaginary part of the permittivity tensor) it is possible to build up the whole spatial distribution at any given wavelength, in particular for X', Y', Z' propagation directions leading to the extrema of the distributions. Because the parameters are wavelength dependent, in particular the off-diagonal element responsible for the distribution rotation, the richness of the lasing ability is enhanced, especially in the field of two-frequency lasing for difference frequency in the THz range.

References

1. DeLoach D.L., Payne A. S., Chase L. L., Smith K. L., Kway W. L., Krupke W. F., *IEEE J. Quant. Electron.* **29**, 1179-1191 (1993).
2. Patel F. D., Honea E. C., Speth J., Payne S. A., Hutcheson R., Equall R., *IEEE J. Quant. Elec*. **37**, 135-144 (2001).
3. Sumida D. S., Betin A. A., Bruesselbach H., Bryen R., Matthews S., Reeder R., Mangir M. S. , *Laser Focus World* **35**, 63-70 (1999).
4. Goldberg L., McIntosh C., Cole B. , *Opt. Expr.* **19**, 4261-4267 (2011).
5. Hugel H. , Opt. Las. Engin. **34**, 213-229 (2000).
6. Brunner F. et al. , Opt. Lett. **27**, 1162-1164 (2002).
7. J. Akiyama, Y. Sato, and T. Taira., Opt. Lett., **35**, 3598 (2010).
8. Hellstrom J. E. et al. , Laser physics **17**, 1204-1208 (2007).
9. Major A., Sandkuijl D. and Barzda V. A , Laser Phys. Lett. **6**, 779-781 (2009).
10. Brenier A., Tu C., Zhu Z., Li J**.** , Appl. Phys. Lett., **90**, 071103-3 (2007).
11. Brenier A., IEEE J. Quant. Electr. **47**, 279-284 (2011).
12. Brenier A. , Las. Phys. Lett. **8**, 520-254 (2011).
13. Tani M., Gu P. , Hyodo M., Sakai K., Hidaka T. , Opt. Quant. Electron. **32**, 503-520 (2000).
14. Sakai K. *Terahertz Optoelectronics* (Springer-Verlag Berlin Heidelberg, 2005).
15. Kh. Kitaeva G. Kh. Laser Phys. Lett. **5**, 559-576 (2008).
16. Tanabe T. , Suto K. , Nishizawa J.-I., Sasaki T. J. , Phys. D: Appl. Phys. **37**, 155-158 (2004).
17. Ding Y. J. , IEEE J. Select. Top. Quant. Electron. **13**, 705-720 (2007).
18. Ding Y. J., Jiang Y., Xu G.and Zotova I. B. Laser Phys. **20**, 917-930 (2010).
19. Muller A., Faist J. , Nature Photonics **4**, 291-291 (2010).

20. Koch M. , *Opt. Photon. News* **18**, 21-25 (2007).

21. Duling I. and Zimdars D. , *Laser Focus World* **43**, 63-69 (2007).

22. Voigt W. , Phil. Mag. S. 6, **4**, 90-97 (1902).

23. Pancharatnam S. , Proc. Ind. Acad. Sci. A, **40 A**, 196-210 (1954).

24. Agranovitch V. M., Ginzburg V. L. *Crystal optics with spatial dispersion, and excitons,* (Springer-Verlag, Berlin Heidelberg New-York Tokyo 1984).

25. Petit Y., Boulanger B., Segonds P., Félix C., Ménaert B., Zaccaro J., G. Aka G. , Opt. Express **16**, 7997-8002 (2008).

26. Joly S., Petit Y., Boulanger B., Segonds P., Félix C., Ménaert B., Aka G. , Opt. Express **17**, 19868-19873 (2009).

27. Brenier A., Wu Y., Zhang J., Fu P., J. Appl. Phys. **108**, 093101-3 (2010).

28. Y. Petit, S. Joly, P. Segonds, B. Boulanger, Laser Phys. **21**, 1305-1312 (2011).

29. Jing F., Wu Y., Fu P. , J. Cryst. Growth **285,** 270-274 (2005).

30. Zhang J., Wu Y., Zhang G., Zu Y., Fu P., Wu Y. , Crystal Growth and Design **10,** 1574-1577 (2010).

31. Gerardin J. Lakhtakia A. , Optik **112**, 493-495 (2001).

32. McCumber D. E. , Phys. Rev. **136**, 954-957 (1964).

33. Jing F., Fu P., Wu Y., Zu Y., Wang X. , Opt. Mater. **30**, 1867-1872 (2008).

34. A. Majchrowski, A. Mandowska, I. V. Kityk, J. Kasperczyk, M. G. Brick, I. Sildos, Curr. Op. Sol. State and Mat. Science, **12**, 32 (2009).

35. A. H. Reshak, S. Auluk, I. V. Kityk, Phys. Rev. B **75**, 245120 (2007).

Acknowledgments

This work was partially supported by the French Agence Nationale de la Recherche (grant n° BLAN06-1_140754) and by the National Basic Research Project of China (n° 2010CB630701).

Figure captions

1. (a) X, Y, Z-polarized absorption spectra,

(b) Off-diagonal element of the absorption permittivity tensor in the X, Y, Z dielectric frame,

of the 15% Yb^{3+} doped $La_2CaB_{10}O_{19}$ crystal. The θ_0 angle is calculated at wavelengths marked out by the arrows.

2. (a) X, Y, Z-polarized emission spectra of Yb^{3+}: $La_2CaB_{10}O_{19}$.

(b) Off-diagonal element of the emission permittivity tensor in the X, Y, Z dielectric frame of an amplifying Yb^{3+}: $La_2CaB_{10}O_{19}$ sample with an excited-state population fixed at one tenth of the 15% doping. The θ_0 angle is calculated at wavelengths marked out by the arrows.

3. (a) Absorption spectra

(b) Emission spectra

of the extraordinary waves propagating in the XZ principal plane in two quasi-symmetrical directions in respect to the Z-axis.

4. (a) Spatial distribution of the stimulated emission cross-section of the a-mode at 1029.6 nm. The (θ, ϕ) direction of propagation is marked out by the orthogonal projection on the XZ principal plane of the (θ, ϕ) direction unit vector.

(b) intensity (arbitrary units) in polar coordinates of the extraordinary emission in the XZ-principal plane. The fours circles on the theoretical blue line are experimental data.

5. 5. (a) Spatial distribution of the stimulated emission cross-section of the b-mode at 1029.6 nm. The (θ, ϕ) direction of propagation is marked out by the orthogonal projection on the XZ principal plane of the (θ, ϕ) direction unit vector.

(b) intensity (arbitrary units) in polar coordinates of the ordinary emission in the XZ-principal plane. The circle on the theoretical blue line is an experimental data.

6. Laser intensities of the ordinary (Y-polarized) mode and extraordinary (XZ-polarized) mode in two directions of propagation in the XZ principal plane:

(a) at θ=-37.4° polar angle

(b) at θ=37.0° polar angle

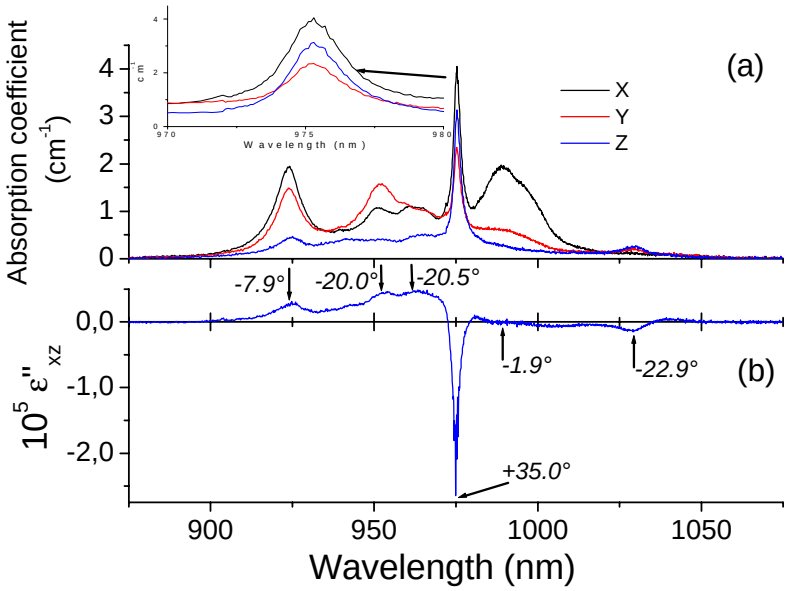
Absorption coefficient (cm-1)
(a)
X
Y
Z
Wavelength (nm)
-7.9°
-20.0°
-20.5°
-1.9°
-22.9°
+35.0°
(b)
10^5 ε" xz
Wavelength (nm)

Fig 1

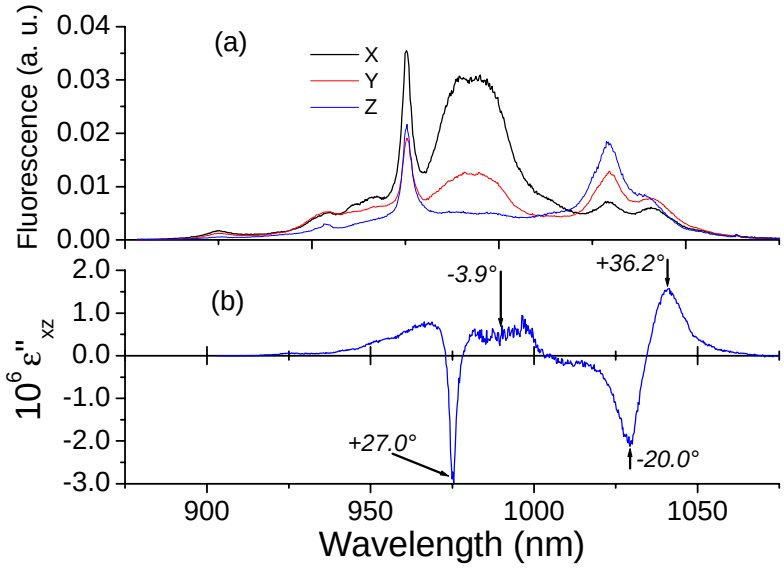
(a)
X
Y
Z
Fluorescence (a. u.)
0.04
0.03
0.02
0.01
0.00
(b)
-3.9°
+36.2°
+27.0°
-20.0°
$10^6 \varepsilon''_{xz}$
2.0
1.0
0.0
-1.0
-2.0
-3.0
900
950
1000
1050
Wavelength (nm)

Fig 2

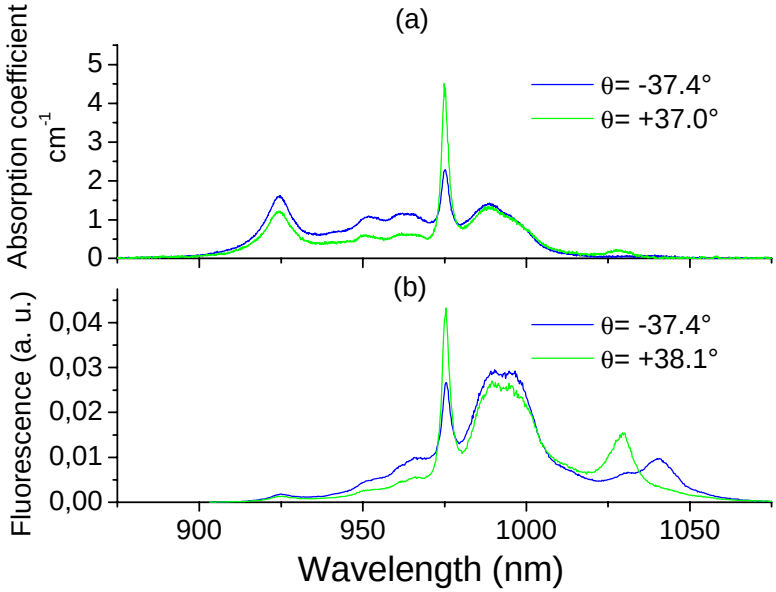
(a)
Absorption coefficient
cm-1
5
4
3
2
1
0
θ= -37.4°
θ= +37.0°
(b)
Fluorescence (a. u.)
0,04
0,03
0,02
0,01
0,00
θ= -37.4°
θ= +38.1°
900
950
1000
1050
Wavelength (nm)

Fig 3

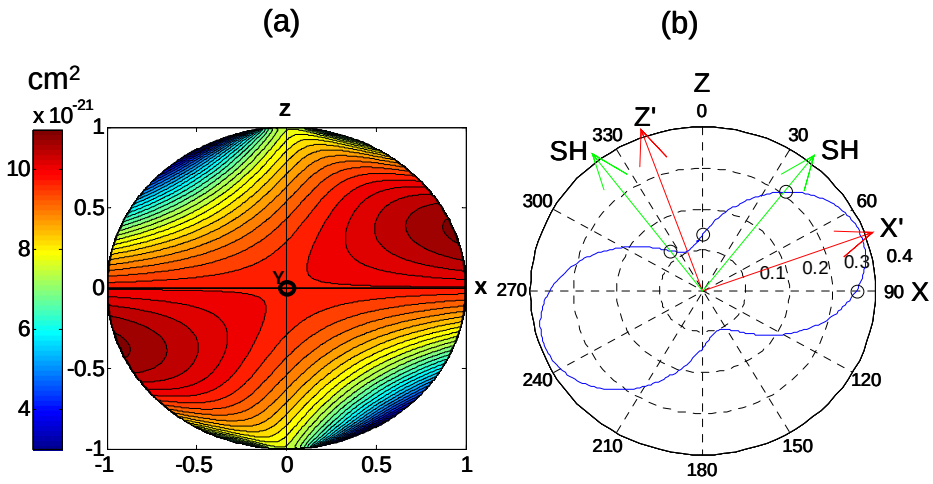
(a)
(b)
cm2
x 10-21
10
8
6
4
z
1
0.5
0
-0.5
-1
y
x
-1
-0.5
0
0.5
1
Z
Z'
SH
SH
X'
X
0
30
60
90
120
150
180
210
240
270
300
330
0.1
0.2
0.3
0.4

Fig 4

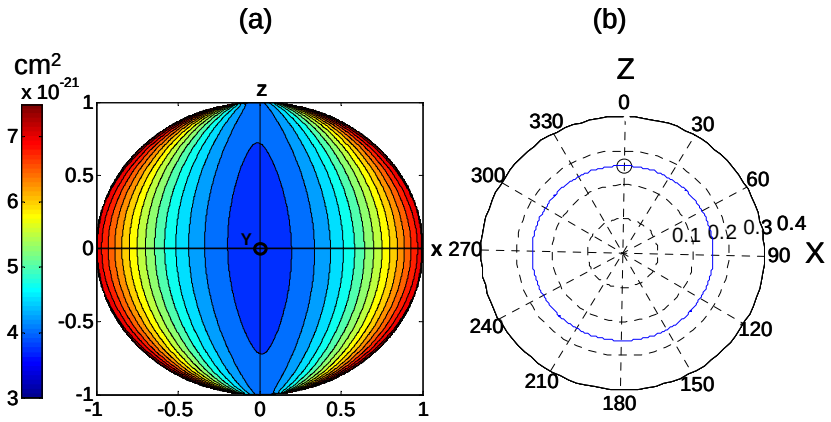
(a)
(b)
cm²
x 10⁻²¹
7
6
5
4
3
z
Y
x
1
0.5
0
-0.5
-1
-1
-0.5
0
0.5
1
Z
X
0
30
60
90
120
150
180
210
240
270
300
330
0.1
0.2
0.3
0.4

Fig 5

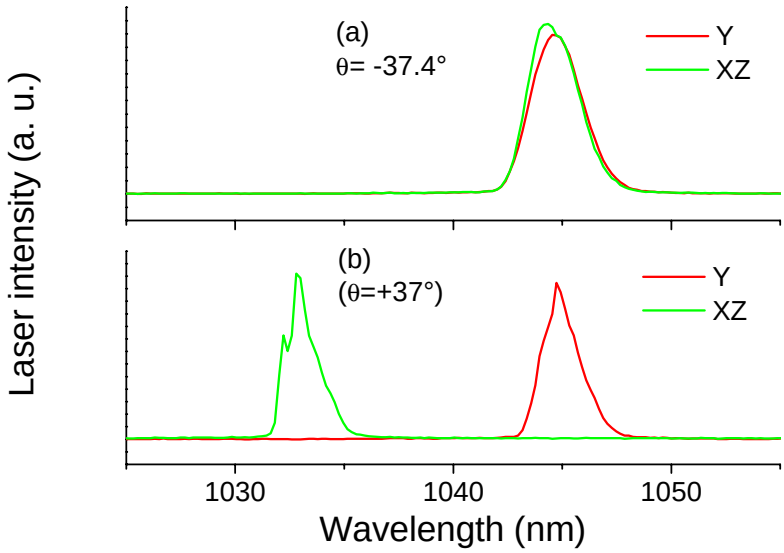
(a)
θ= -37.4°
Y
XZ
(b)
(θ=+37°)
Y
XZ
Laser intensity (a. u.)
1030
1040
1050
Wavelength (nm)

Fig 6